Strain-phonon coupling in (111)-oriented perovskite oxides

*Magnus Moreau,[1] Astrid Marthinsen,[2] Sverre M. Selbach,[2] and Thomas Tybell[1,]**

1) Department of Electronic Systems, NTNU Norwegian University of Science and Technology, 7491 Trondheim, Norway

2) Department of Materials Science and Engineering, NTNU Norwegian University of Science and Technology, 7491 Trondheim, Norway

*E-mail: thomas.tybell@iet.ntnu.no

ABSTRACT

Strain-phonon coupling, in terms of the shift in phonon frequencies under biaxial strain, is studied by density functional theory calculations for twenty perovskite oxides strained in their (111)- and (001)-planes. While the strain-phonon coupling under (001)-strain follows the established, intuitive trends, the response to (111)-strain is more complex. Here we show that strain-phonon coupling under (111)-strain can be rationalized in terms of the Goldschmidt tolerance factor and the formal cation oxidation states. The established trends for coupling between (111)-strain and in-phase and out-of-phase octahedral rotational modes as well as polar modes provide guidelines for rational design of (111)-oriented perovskite thin films.

INTRODUCTION

Perovskite oxides, with general formula ABO_3, are known for their strong structure property coupling, making them susceptible to external stimuli. Hence, synthesis of epitaxial thin films on substrates with different lattice parameters open for strain engineering of physical properties. Strain engineering in the (001)-plane has e.g. been utilized to induce ferroelectricity in $SrTiO_3$ (STO), effectively transforming the system from a paraelectric state with out-of-phase octahedral rotations in $I4/mcm$ symmetry, represented by Glazer tilt system $a^0a^0c^-$,[1] to a ferroelectric state with $P4mm$ symmetry.[2,3] (001)-strain has further enhanced the Curie temperature and polarization in $BaTiO_3$ (BTO)[4] or induced multiferroicity in $SrMnO_3$ (SMO).[5] These strain-induced changes of functional properties are often linked to certain phonon modes, which either condense or have their amplitudes altered by the imposed strain. Important phonon modes for functional properties of perovskite oxides include rotations/tilts of the oxygen octahedra and polar cation displacements. Strain-phonon coupling, the effect of strain on the phonon modes, has been much studied for (001)-strain over the last decades.[3,6-12] As shown in Figure 1, it has been established for octahedral rotations that compressive (001)-strain softens rotations around the out-of-plane axis, while tensile (001)-strain softens rotations around the in-plane axes.[6-8,10,11] Similarly, out-of-plane polar modes are softened under (001)-compression, while in-plane polar phonon modes are softened under tensile (001)-strain.[2-4,9,10,12]

An interesting proposition is to rely on higher index surfaces such as (111),[13] because its structure resembles a buckled honeycomb lattice similar to 2D materials, giving prospect for novel topological properties.[14] It has been shown experimentally that (111)-compression in rare earth nickelates ($R$$NiO_3$) can result in a polar metal,[15] (111)-strain of $PbTiO_3$ grown on $LaAlO_3$ (LAO) (111)-substrates displayed complex dislocations different to what is expected for low index interfaces,[16] and compressive (111)-strain in $BiFeO_3$ results in a mono-domain polar phase.[17] In addition, theoretical studies of strain in the (111)-plane has revealed different response of the octahedral rotations in LAO[18] and the polar modes of BTO[19] and $PbTiO_3$,[20] as compared to (001)-strain. Furthermore, in-plane octahedral rotations in LAO under compressive (111)-strain has been shown to exhibit a Goldstone-like behavior.[18] Finally, we note that a mismatch between out-of-phase and in-phase octahedral rotations across an interface can induce

novel magnetic states,[21] which can induce a magnetic moment without charge transfer in (111)-oriented thin films.[22] Thus understanding general trends for how (111)-strain affects phonon frequencies, and developing routes to tailor soft and hard phonon modes in a material, is essential for rational design of new functional materials for electronic and spintronic applications.

In order to advance the overall understanding of the interplay between epitaxial strain, applied to (111)-oriented thin films, and octahedral rotations and polar modes, we present a density functional theory (DFT) study of the (111)-strain response of phonon frequencies for a large number of perovskite oxides. Results for (001)-strain are also presented for comparison. Data are presented for III-III, II-IV, and I-V perovskite systems, focusing mainly on d^0 or d^{10} materials to minimize effects from magnetism and strongly correlated electrons. However, the general trends presented should still be valid for other number of d electrons,[23,24] as demonstrated here for the d^5 material $LaFeO_3$ (LFO). It is shown that the result of phonon-strain coupling for (111)-strain can be related to the Goldschmidt tolerance factor[25] t describing the size mismatch between the A- and B-cation. Furthermore, while (001)-strain typically affects in-phase and out-of-phase rotations similarly, this is not the case for (111)-strain.

The article is structured as follows: first, the methodology including the calculation details is presented, before two examples are given to highlight the difference in phonon response for (001)- and (111)-strain. Finally, the general results for (111)-strain on relevant phonon modes are presented, emphasizing the effect on octahedral rotations and polar displacements of the B-cations.

METHODOLOGY

This work focuses on three different types of modes, at different locations in the Brillouin zone, which have all been shown to be important for different functional properties of perovskite oxides.[6] These modes are: out-of-phase octahedral rotations, where every second layer along the rotation rotates in the opposite direction, centered at the $R = (\frac{1}{2}, \frac{1}{2}, \frac{1}{2})$ point (Figure 2 a)), in-phase rotations, where every second layer along the rotation axis rotates in the same direction, centered at the $M = (\frac{1}{2}, \frac{1}{2}, 0)$ point (Figure 2 b)), and polar displacements of the B cation at the $\Gamma = (0,0,0)$ point (Figure 2 c)). For a cubic perovskite, each mode is triply degenerate. However, under quadratic in-plane strain they are typically

split into two degenerate in-plane modes and one out-of-plane mode.[18] For (001)-strain the out-of-plane modes have rotation or polar axis along [001], while it has in-plane axes along [100] and [010], as shown in Figure 1. On the other hand for (111)-strain the out-of-plane axis is along [111], while the in-plane axes are along the $[1\bar{1}0]$ and $[11\bar{2}]$ directions. Hence, while the in-plane modes for (001)-strain has the same symmetry, this is not the case for (111)-strain.[18] All crystallographic directions are given in the pseudocubic setting, unless otherwise stated.

To understand the general trends of these modes under strain, the phonon frequencies have been calculated for systems with different tolerance factors and oxidation states of the A and B cations. Since the compressibility of the cations are significantly different for III-III, II-IV and I-V perovskites, the effect of the oxidation state is also considered.[26] The calculations were performed for both (001)- and (111)-strain, in order to elucidate possible differences between these two strain planes. The III-III perovskites studied in this work are, (ground state space group in parenthesis): LAO ($R\bar{3}c$[27]) $NdAlO_3$ (NAO, $R\bar{3}c$[28]), $LaGaO_3$ (LGO, $Pnma$[29,30]) LFO ($Pnma$[31]), $YAlO_3$ (YAO, $Pnma$[32]) $GdScO_3$ (GSO, $Pnma$[30]) and $DyScO_3$ (DSO, $Pnma$[33]). The II-IV perovskites include BTO ($R3m$[34]) STO ($I4/mcm$[35]) $BaZrO_3$ (BZO, $Pm\bar{3}m$[36]), $CaTiO_3$ (CTO, $Pnma$[37]) and $SrZrO_3$ (SZO, $Pnma$[38]). While the I-V perovskites studied in this work are $KNbO_3$ (KNO, $R3m$[39]), $KTaO_3$ (KTO, $Pm\bar{3}m$[40]), $NaTaO_3$ (NTO, $Pnma$[41]), $NaNbO_3$ (NNO, coexisting $R3m$ and $Pbcm$ phases[42]), and $AgNbO_3$ (ANO, $Pmc2_1$[43]). In addition, the materials $MgTiO_3$ (MTO, $R\bar{3}$[44]) and $LiNbO_3$ (LNO, $R3c$[45]), which are only metastable in a perovskite phase, were also analyzed as perovskites in order to extend trends for II-IV and I-V materials to t below 0.9. In order to take into account that these twenty different perovskites crystalize in different space groups with different levels of distortions, the methodology by Hong et al.[24] were employed. This method consists of analyzing changes in phonon frequencies in a highly symmetric phase. This phase has cubic $Pm\bar{3}m$ symmetry when the material is unstrained, while under (001)-strain it becomes tetragonal with $P4/mmm$ symmetry and under (111)-strain it becomes rhombohedral with $R\bar{3}m$ symmetry.

The DFT calculations were done with the Vienna Ab-initio Simulation Package (VASP, version 5.3.3)[46,47] employing the projector augmented wave method (PAW).[47,48] The Perdew-Burke-Ernzerhof

generalized gradient approximation for solids (PBEsol) was chosen as it has been shown to accurately reproduce the crystal structure and lattice parameters of solids.[49] The different material systems were first relaxed in the high symmetry, cubic $Pm\bar{3}m$ phase using $1 \times 1 \times 1$ cells. The only exception to this is LFO, were a $2 \times 2 \times 2$ supercell was used in order to properly account for G-type antiferromagnetism.[50] As shown in Figure 2 d), for (001)-strain the unit cells was arranged such that the $\boldsymbol{a}$ and $\boldsymbol{b}$ lattice vectors, pointing along the in plane $[100]$ and $[010]$ direction respectively, were fixed, while the $\boldsymbol{c}$ lattice vector, which is along the out-of-plane $[001]$ direction, was allowed to relax.[8] As shown in Figure 2 e), for (111)-strain the calculation cells were rotated with the following rotation matrix:

$$R = \begin{bmatrix} 1 & 0 & 1 \\ \bar{1} & 1 & 1 \\ 0 & \bar{1} & 1 \end{bmatrix}, \qquad (1)$$

such that the $\boldsymbol{a}$ and $\boldsymbol{b}$ lattice vectors were along $[1\bar{1}0]$- and the $[01\bar{1}]$-pseudocubic directions respectively, while the $\boldsymbol{c}$ lattice vector was along the $[111]$-direction. With this configuration, the (111)-strain could be introduced by fixing in the effective **a** and **b** lattice vectors while the cell was allowed to relax along the **c** lattice vector. The minimal unit cell for the (111)-strain calculations is a $\sqrt{2} \times \sqrt{2} \times \sqrt{3}$ supercell containing 15 atoms, while a $\sqrt{2} \times \sqrt{2} \times 2\sqrt{3}$ cell containing 30 atoms, is needed to include the G-type antiferromagnetism of LFO.

The plane-wave energy cutoff was set to 550 eV for all calculations, except the ones including Li, where it was increased to 650 eV. For the $1 \times 1 \times 1$ cells an $8 \times 8 \times 8$ Γ-centered k-point mesh was used, while a $6 \times 6 \times 5$ mesh was used for the $\sqrt{2} \times \sqrt{2} \times \sqrt{3}$ cells used for (111)-strain calculations. Corresponding k-point densities were used for the supercells. The electronic structure was minimized until the energy difference between two steps were smaller than 10^{-9} eV, while the ionic optimization was minimized until the energy difference between two subsequent steps was smaller than 10^{-8} eV. The recommended PAW potentials supplied with the VASP package[51] were used for Li, Na, K, Mg, Ca, Sr, Ba, Sc, Y, La, Nd, Gd, Dy, Ti, Zr, Nb, Ta, Fe, Ag, Al, Ga, and O. These have electronic configurations $1s^2 2s^1$, $2p^6 3s^1$, $3s^2 3p^6 4s^1$, $3s^2$, $3s^2 3p^6 4s^2$, $4s^2 4p^6 5s^2$, $5s^2 5p^6 6s^2$, $3s^2 3p^6 3d^1 4s^2$, $4s^2 4p^6 4d^1 5s^2$, $4s^2 4p^6 4d^1 5s^2$,

$4p^6 5d^1 6s^2$, $4p^6 5d^1 6s^2$, $3s^2 3p^6 3d^2 4s^2$, $4s^2 4p^6 4d^2 5d^2$, $4s^2 4p^6 4d^3 5s^2$, $5p^6 5d^3 6s^2$, $3p^6 3d^6 4s^2$, $4d^9 5s^2$, $3s^2 3p^1$, $3d^{10} 4s^2 4p^1$, and $2s^2 2p^4$, respectively. Hence, the f electrons were treated as core electrons for Nd, Gd and Dy. The GGA+U approach as introduced by Dudarev et al.[52] was used for La f-states and the Fe d states with a U-value of 10 and 3 eV respectively.[11] Phonon calculations were performed utilizing the frozen phonon approach[53] and analyzed with the phonopy software.[54] The phonon calculations were done in $2 \times 2 \times 2$ supercells, and it was confirmed that all phonon calculations resulted in three degenerate acoustic modes at approximately zero frequency.

Two different measures are introduced to quantify the effect of strain on phonon structure, Δf the frequency difference between in-plane and out-of-plane modes, and $\mathrm{d}f/\mathrm{d}\epsilon$, the derivative of the phonon frequency with respect to strain. The frequency difference between in-plane and out-of-plane modes is defined as

$$\Delta f = \begin{cases} f_{\parallel} - f_{\perp} & \text{if } \epsilon < 0 \\ f_{\perp} - f_{\parallel} & \text{if } \epsilon > 0 \end{cases}, \qquad (2)$$

where $f_{\parallel}$ and $f_{\perp}$ are the frequencies of the in-plane and out-of-plane modes respectively. Here, ϵ is the strain with respect to the high symmetric cubic phase defined as $\epsilon = (a - a_0)/a_0$, where a_0 is the relaxed lattice parameter in the cubic $Pm\bar{3}m$ phase. As illustrated in Figure 1, this definition of Δf ensures that changing the sign of ϵ does not change the sign of Δf, and that Δf is positive for (001)-strain for the modes considered here. In this work Δf is evaluated at ± 1 % strain, and the average value is presented; this value is chosen to minimize numerical errors that can take place close to zero strain in the calculations, and to ensure that non-linear effects prominent large levels of strain is minimized. $\mathrm{d}f/\mathrm{d}\epsilon$ is taken as a measure of how susceptible a phonon mode is to be destabilized by strain. $\mathrm{d}f/\mathrm{d}\epsilon$ is evaluated at $\epsilon \approx 0$, hence a positive (negative) $\mathrm{d}f/\mathrm{d}\epsilon$ corresponds to a mode being softened by compressive (tensile) strain. While Δf directly compares the in-plane and out-of-plane modes of the same type, $\mathrm{d}f/\mathrm{d}\epsilon$ is more suitable when comparing different types of modes. Illustration of the atomic structures were made with VESTA.[55]

RESULTS

Lattice parameters and Poisson's ratios

The effect of strain is closely coupled to the Poisson's ratio of a material. In Table I the relaxed lattice parameters of the aristotype cubic phase, as well as calculated Poisson's ratios, ν, for (001)- and (111)-strain are presented. Under a given amount of strain, the ν will determine the amount of strain in the high-symmetry phases, for discussion about the effect see supplementary information.[56] The overall trend for ν is opposite for systems under (001)- and (111)-strain. $\nu_{(001)}$ increases for increasing tolerance factor, while $\nu_{(111)}$ is reduced for increasing tolerance factor. For materials with similar t but with different oxidation states, $\nu_{(001)}$ goes from largest to smallest in the order of III-III, II-IV and I-V, while for $\nu_{(111)}$ it goes from largest to smallest in the opposite order, I-IV, II-IV and III-III. This can be rationalized from the difference in compressibility of the A-O and B-O bonds for III-III, II-IV and I-V perovskites respectively.[26] In the case of (001)-strain, the strain is parallel to the in-plane B-O bonds, while for (111)-strain the strain it is parallel to the in-plane A-O bonds (see Figure 2 d-e). Hence, for (001)-strain the compressibility of the B-O bonds are dominating and lowest for I-V perovskites, while for (111)-strain it is the compressibility of the A-O bonds, largest for I-V perovskites, that is the most important.[26] Deviations from these trends are observed from materials with different electron configurations, such as LFO for III-III perovskites, the difference between Ti and Zr in II-IV perovskites, and ANO for I-V perovskites.

We now exemplify the introduced measures, Δf and $df/d\epsilon$, through two materials either susceptible to polar instabilities, STO, or rotational instabilities, NTO. Corresponding data for the other material systems are given in the supplementary information, Figure S2-S19.[56]

Example 1: II-IV $SrTiO_3$, t = 1.001

STO, having a tolerance factor close to unity,[35,57] exhibit a large strain-phonon coupling,[2,3] and could in principle condensate any of the three different types of phonon modes studied here. In order to calculate Δf and $\mathrm{d}f/\mathrm{d}\epsilon$, the phonon frequencies for the central modes are calculated as a function of both (001)- and (111)-strain. At 0 % strain, STO have both imaginary out-of-phase rotations and polar modes, while

the in-phase rotations are real, but relatively low in frequency (0.58 THz). For (001) type strain, compressive strain softens rotational modes around the out-of-plane axis and out-of-plane polar modes, while tensile strain softens rotational modes around the in-plane axis and in-plane polar modes, as shown in Figure 3 a). Based on the data, a positive Δf is deduced for all three kinds of modes under (001)-strain, as expected from the definition of Δf.[2,7] For (111)-strain on the other hand, different trends are observed. It is shown in Figure 3 b for the out-of-phase rotations that STO follows the same trend as was found for LAO,[18] in-plane rotations around the $[1\bar{1}0]$ sand $[11\bar{2}]$ are softened under compressive strain while out-of-plane rotations around $[111]$ are softened for tensile strain, resulting in a negative Δf_{rot-}. In contrast to the case for (001)-strain, (111)-strain does not split the in-phase rotations into two in-plane components and one out-of-plane component. Instead, the three in-phase rotations are degenerate for all (111)-strain values, i.e. $\Delta f_{rot+} = 0$. However, (111)-strain changes the frequencies of the in-phase rotations, which for STO become imaginary at compressive strain. Thus depending on the competition between the other modes, the in-phase rotations could condensate, as has been shown experimentally for (001)-strained $La_{1-x}Sr_xMnO_3$.[58] Finally, the polar modes follow the same trend as was earlier deduced for BTO under (111)-strain,[19,20] having both the in-plane and out-of-plane polar modes softened for tensile strain, i.e. $\mathrm{d}f_{pol}/\mathrm{d}\epsilon_{(111)} < 0$ for both in-plane and out-of-plane modes. Thus, by compressively straining STO in the (111)-plane, any ferroelectric instability will be suppressed; while by increasing (111)-tension in STO one could condense both an in-plane and an out-of-plane polarization component.

Example 2: I-V $NaTaO_3$, t = 0.968

NTO, having a bulk $Pnma$ symmetry[41] with an $a^-b^+a^-$ Glazer tilt pattern,[1] has a tolerance factor, $t = 0.968$[57] and is thus prone to octahedral rotations and tilts. The phonon frequencies are plotted as a function of (001)- and (111)-strain in Figure 4. As seen, for 0 % strain both the in-phase and out-of-phase rotations have a large imaginary frequency. Based on this, both modes are expected to condensate, consistent with the $a^-b^+a^-$ bulk tilt pattern. For (001)-strain, depicted in Figure 4 a), NTO follows the same trends as STO, for compressive (001)-strain out-of-plane rotational and polar modes are softer, while for tensile (001)-strain the in-plane rotational and polar modes are softer. Hence, in line with the

definition, all modes have a positive Δf. From the calculated phonon frequencies as a function of strain it is inferred that both the in-plane and out-of-plane rotations have a positive $df_{rot\pm}/d\epsilon$ for both (001) and (111) strain. This can be understood by the low compressibility of the B-O bonds in I-V perovskites, and that the volume is reduced (increased) under compressive (tensile) strain making rotations softer (harder). Furthermore, we see that, similar to STO, the polar modes exhibit larger positive $\mathrm{d}f/\mathrm{d}\epsilon$ than the rotational modes under (001)-strain, pointing towards a polar transition under sufficiently large strain. However, while NTO follows the same trends as STO for (001)-strain, the response to (111)-strain is considerably different (Figure 4b). The splitting of out-of-phase modes are not reversed for (111)-strain with respect to (001)-strain. For NTO the out-of-plane out-of-phase rotations are preferred for compressive strain, while in-plane out-of-phase rotations are preferred for tensile strain, i.e. Δf_{rot-} is positive, similar to (001)-strain. For the polar modes, $\mathrm{d}f/\mathrm{d}\epsilon$ for the out-of-plane polarization is similar to what is observed for (001)-strain, hence $\mathrm{d}f_{pol\perp}/\mathrm{d}\epsilon_{(111)} > 0$ at zero strain. However, for tensile strain values larger than 2 % it saturates, and shifts sign. As $df_{rot\pm}/d\epsilon_{(111)} > 0$ and $d_{pol}/d\epsilon_{(111)} < 0$ for $\epsilon > 2\%$, a ferroelectric transition is also expected at about 3-4 % tensile strain. The shift in sign of $\mathrm{d}f_{pol\perp}/\mathrm{d}\epsilon_{(111)}$ is consistent with the polar modes having fewer symmetry restrictions than the rotational modes, this since both the A- and B cations can contribute to the displacement. This contributes to a more non-linear frequency-strain response of the polar modes as compared to the rotational modes. For compressive (111)-strain the displacement is more dominated by A-sites than B-sites (see Figure S20 in supplementary information[56]), in agreement with BTO under hydrostatic pressure.[59]

Overview of the strain-phonon coupling in the (111)-orientation

As discussed in the previous sections, STO and NTO, has significant different strain phonon couplings, in disagreement with (001)-strain for which there is a universal strain response.[6] In analogy to Figure 1, which summarizes the strain-phonon coupling for (001) strain, we present an overview of the strain-phonon coupling for (111)-strain in Figure 5 clearly displaying a different strain response as compared to (001)-strain. The tolerance factor, t, a measure of stress on the A-O and B-O bonds in the unstrained $Pm\bar{3}m$ phase, is taken as a control parameter.[60] As shown in Figure 5, for low tolerance factors (~ 0.9), the strain-phonon coupling in the (111)-plane for out-of-phase rotations and polar modes is similar to

what is observed for (001)-strain, i.e $\Delta f_{rot-} > 0$, and $df_{pol,\perp}/d\epsilon_{(111)}$ and $df_{pol,\parallel}/d\epsilon_{(111)}$ has the opposite sign. In contrast, for larger tolerance factors (~ 1.0), the out-of-phase rotations display opposite splitting compared to (001)-strain. The in-plane and out-of-plane polar modes have the same sign, hence affected in the same manner for both compressive and tensile strain, i.e. $\Delta f_{rot-} < 0$, and $df_{pol,\perp}/d\epsilon_{(111)}$ and $df_{pol,\parallel}/d\epsilon_{(111)}$ have the same sign. Finally, in-phase rotations are not split under (111)-strain regardless of tolerance factor.

In the following sections, we confirm these trends by analyzing all the twenty different oxides. Furthermore, we show that the exact tolerance factor where these changes in strain phonon coupling occur is sensitive to the oxidation state of the A and B cations.

Out-of-phase rotations

The two measures introduced above (Δf and $df/d\epsilon$) will now be used to analyze trends for rotational and polar modes in various perovskites under (111)-type strain. First the out-of-phase rotational modes (illustrated in Figure 2 a) are analyzed. Such modes were shown to have an inverse splitting between in-plane and out-of-plane modes between (001)- and (111)-strain for STO and LAO,[18] but not for NTO. In Figure 6, Δf_{rot-} vs. tolerance factor is shown for the materials considered in this study. For (001)-strain Δf_{rot-} is always positive (Figure 6a), however Δf_{rot-} is reduced with reducing tolerance factor approaching zero for t less than 0.9. Thus, for all the materials studied here, out-of-plane rotations are softer for compressive (001)-strain and in-plane rotations are softer for tensile strain as expected.

For (111)-strain a different trend is observed (Figure 6b). When the tolerance factor is approximately unity Δf_{rot-} is negative, i.e. in-plane rotations are softer for compressive strain and out-of-plane rotations are softer for tensile strain. However, as the tolerance factor is reduced, Δf_{rot-} changes sign. The critical tolerance factor where this change occurs appears to be largest for I-V perovskites and lowest for III-III perovskites. However, no clear monotonic trend in the Δf_{rot-} as a function of tolerance factor can be inferred.

To better understand this tolerance factor dependence of Δf_{rot-} an analysis of how the derivative of phonon frequencies change as a function of strain at 0 % strain is presented. The evolution of $df_{rot-}/d\epsilon$

with tolerance factor for in-plane modes for (001)-strain and out-of-plane modes for (111)-strain is depicted in Figure 7. As can be seen, there is a clear trend with increased Δf_{rot-} values for lower tolerance factors and lower oxidation states of the A-cation. The different oxidation states, represented by different colors, have each an almost linear dependence with tolerance factor. However, when analyzing the derivatives for the out-of-plane modes for (001)-strain and the in-plane modes for (111)-strain no such clear trend is found, as shown in Figure 8.

Three materials, STO, BZO and ANO are deviating from the trends discussed above. Interestingly these same materials deviate from the trend for both (001)-strain and (111)-strain. For STO and BZO the deviations in the derivative of the out-of-plane rotations for (001)-strain and in-plane rotations for (111)-strain is consistent by the fact that these two materials both have a tolerance factor very close to unity. When the tolerance factor is unity (1 ± 0.005) the cubic phase with degenerate phonon modes becomes a stable, and a small amount of strain can then result in destabilization of different modes. This is consistent with the increase of the $df/d\epsilon$ values for STO and BZO. For ANO on the other hand, it is the fact that ANO has a significantly larger Poisson's ratio (table I) than the other I-V Perovskites. A larger Poisson's ratio increases the octahedral distortions (see supplementary information, Figure S1[56]), and hence weakens the coupling between the strain and the phonon frequencies.

Combining these results, the change in sign of the splitting Δf_{rot-} for (111)-strain can be rationalized by the AO_3 + B + AO_3 + B + … stacking along the (111)-direction, as shown in Figure 2 e). For large tolerance factors the A-cation and the oxygen atoms are in the same plane, hence a negative Δf_{rot-}. The exact crossover point from negative to positive Δf_{rot-} depends on the oxidation state as shown in Figure 6 b). Under compressive (tensile) strain the oxygen atoms are closer to (further away from), the A cation, hence the A-cation is forcing the oxygen atoms to rotate in-plane (out-of-plane) to optimize its coordination. However, when the A-cation is smaller (i.e. reduced tolerance factor), the elastic forces it exerts on the oxygen atoms are reduced and Δf_{rot-} becomes positive in-line with what is expected for (001)-strain. Similarly, when the oxidation state of the A cation is lowered, the force it exerts on the oxygen atoms is reduced. Hence, this geometric argument is consistent with Δf_{rot-} changing sign for largest t for I-V perovskites, intermediate t for the II-IV perovskites and lowest t for III-III perovskites

(Figure 7). There is also a duality between in-plane modes for (001)-strain and out-of-plane modes for (111)-strain, which follow the trends, and a similar duality between out-of-plane modes for (001)-strain and in-plane modes for (111)-strain which does not follow a given trend.

In-phase rotations

The in-phase rotational modes (illustrated in Figure 2 b) were not split by (111)-strain for STO (Figure 3b) nor NTO (Figure 4b), i.e. $\Delta f_{rot+} = 0$. Under (111)-strain Δf_{rot+} was in fact found to be zero for all materials considered in this study, hence no splitting of in-phase rotations is found. The observation that $\Delta f_{rot+} = 0$ for all perovskites under quadratic (111)-strain can be understood from a symmetry argument. Any in-phase or un-tilted system requires a mirror plane perpendicular to the rotations axis,[1] and these mirror planes are removed as the pseudocubic cell angle α_{pc} (see supplementary information, Figure S1[56]) deviates from 90 degrees.

Even though the splitting is zero, the derivative of the phonon frequencies is still of importance, as that determines if the modes become more or less destabilized by the applied strain. In Figure 9 the derivative of the in-phase rotations is presented, and $df_{rot+}/d\epsilon$ is reduced with an increasing tolerance factor. An A-cation larger in size will be more sensitive to volumetric changes than a small A-cation, and the octahedra will need to rotate more when the volume is reduced. Hence an increased tolerance factor reduces the slope of the strain-phonon frequency relationship. The trend in Figure 9 is found for the III-III perovskites (blue), and most II-IV (pink) and I-V (cyan) perovskites studied. Once again, the results for STO, BZO and ANO deviate from these trends. STO and BZO have a tolerance factor at approximately unity, making them sensitive to small changes in strain, while ANO has a significantly different Poisson's ratio than the other I-V perovskites; as discussed above. Furthermore, for LNO and MTO it seems that the trends have saturated, as these materials are not stable in the perovskite phase.

Polar modes

The final mode type that is discussed in this work is polar displacements of the B-cations, illustrated in Figure 2 c). As was shown for STO in Figure 3 b), an out-of-plane polarization component is softened for tensile (111)-strain, not for compressive (111)-strain. This at first seems counterintuitive, as it means

that the out-of-plane polarization is reduced when the structure is elongated out-of-plane.[19] However, we note that this trend was not observed in NTO for most strain values (Figure 4b). In Figure 10, the derivative of the out-of-plane polarization frequency around 0 % strain is shown for all the materials studied. As seen in Figure 10 a) all materials follows the expected trend for (001)-strain, [9] where $\frac{df_{pol\perp}}{d\epsilon_{(001)}} > 0$, i.e. out-of-plane polarization is softened by compressive strain. However for (111)-strain, (Figure 10 b), there is a shift in the sign of the derivative of the out-of-plane polarization, going from negative at large tolerance factors and turning positive for lower tolerance factors. The trends seen in Figure 10 are not as clear as those observed for the rotational modes in e.g. Figure 7 with respect to oxidation state. As discussed for NTO, (111)-strain allows for significant movement of both A- and B-cations, hence the lower symmetry requirements for polar modes compared to rotational modes weaken possible trends. In contrast to the out-of-plane modes, the in-plane polar modes follow similar trends for both (001)- and (111)-strain, data given in the supplementary information, Figure S21.[56]

This phenomena of hardening of the out-of-plane polarization under (111)-compression was first found for BTO by Oja et al.[20] and later elaborated on by Raeliarijaona and Fu[19], who explained a negative $\frac{df_{pol\perp}}{d\epsilon_{(111)}}$, by considering the stacking sequence along the [111]-direction (Figure 2 e). They found that under (111)-compression the oxygen atoms occupy the space the B-cation should off-center to, thus suppressing the out-of-plane polarization. This can now be extended to other perovskites with lower tolerance factors. For a material with low tolerance factor, the A-cation is typically small and there is hence more room in the plane for the oxygen atoms to shift position. Hence the reduced tendency for the oxygen atoms to inhibit movement of the B-cation. At a critical value around $t = 0.95$, the elongation (compression) of the out-of-plane lattice parameter under compression (tension) becomes more important, and the $\frac{df_{pol\perp}}{d\epsilon_{(111)}}$ becomes positive, similar to what is observed for (001)-strain.

DISCUSSION AND CONCLUSSION

The strain-phonon coupling of (111)-oriented oxide perovskites depend on both the tolerance factor and the formal valence of the A- and B cations. The fact that (111)-strain have a symmetry induced

difference between out-of-phase and in-phase rotations, which is not seen for (001)-strain, opens up new avenues for tailoring the octahedral response. Such tuning can be of interest for epitaxial perovskite interfaces where two octahedral tilt patterns meet, as a mismatch between octahedral in-phase and out-of-phase rotations have been shown experimentally to have large influence on the magnetic properties.[21,22] Furthermore, the different behavior between in-phase and out-of-phase rotations opens interesting vistas for tuning of perovskite iodides and bromides, where in-phase rotations are more common than in their oxide counterpart.[61] On the other hand, for the polar modes for $t \sim 1$, both the in-plane and out-of-plane polarization is almost equally affected, and compressive (111)-strain suppresses the overall ferroelectricity. Also for (111)-strain, the piezoelectric coefficient $e_{31} = \frac{\Delta P_3}{\epsilon_1} = \frac{\Delta P_\perp}{\Delta \epsilon_{(111)}} \sim \frac{\mathrm{d}f_{pol\perp}}{\mathrm{d}\epsilon_{(111)}}$ is positive for high tolerance factors and becomes negative for lower tolerance factors, while it is always negative for (001)-strain.[19] A positive e_{31} implies that an increasing out-of-plane polarization will actually increase the in-plane strain, not decrease it as expected for (001)-oriented films. Especially interesting in this regard is (111)-strained $KNbO_3$ (see supplementary information, Figure S15[56]), which has $\frac{\mathrm{d}f_{pol\perp}}{d\epsilon_{(111)}} < \frac{\mathrm{d}f_{pol\parallel}}{d\epsilon_{(111)}}$ for all tensile strain values, indicating that the out-of-plane polarization will be the dominant polarization component. A positive e_{31}, should in principle be possible for all materials with a positive $\frac{\mathrm{d}f_{pol\perp}}{d\epsilon_{(111)}}$ in Figure 10 b), however in the III-III perovskites studied here, f_{pol} are in the order of 7 THz or larger, and the absolute value of $\frac{\mathrm{d}f_{pol\perp}}{d\epsilon_{(111)}}$ is too low that such modes condensate under experimentally achievable strain values.

Taken together these results illustrates that the complexity of (111)-strain can be taken as additional tuning parameters both for octahedral rotations and polar distortions of perovskite oxides. This points towards that (111)-strain is an interesting avenue for tailoring both magnetic and ferroelectric properties for functional devices.

Acknowledgements

The Norwegian Metacenter for Computational Science is acknowledged for providing computational resources, Uninett Sigma 2, Project No. NN9301K. TT acknowledges funding through the Research

Council of Norway grant No.231290. We thank Gerhard Henning Olsen for valuable discussions about phonon calculations and Ulrich Aschauer for providing the script for automating the phonopy calculations.

References

[1] A. M. Glazer, Acta Crystallogr. Sect. B **28**, 3384 (1972).
[2] J. H. Haeni, P. Irvin, W. Chang, R. Uecker, P. Reiche, Y. L. Li, S. Choudhury, W. Tian, M. E. Hawley, B. Craigo *et al.*, Nature **430**, 758 (2004).
[3] N. A. Pertsev, A. K. Tagantsev, and N. Setter, Phys. Rev. B **61**, R825 (2000).
[4] K. J. Choi, M. Biegalski, Y. L. Li, A. Sharan, J. Schubert, R. Uecker, P. Reiche, Y. B. Chen, X. Q. Pan, V. Gopalan *et al.*, Science **306**, 1005 (2004).
[5] J. H. Lee and K. M. Rabe, Phys. Rev. Lett. **104**, 207204 (2010).
[6] J. M. Rondinelli and N. A. Spaldin, Adv. Mat. **23**, 3363 (2011).
[7] A. J. Hatt and N. A. Spaldin, Phys. Rev. B **82**, 195402 (2010).
[8] A. T. Zayak, X. Huang, J. B. Neaton, and K. M. Rabe, Phys. Rev. B **74**, 094104 (2006).
[9] N. A. Pertsev, A. G. Zembilgotov, and A. K. Tagantsev, Phys. Rev. Lett. **80**, 1988 (1998).
[10] A. Marthinsen, C. Faber, U. Aschauer, N. A. Spaldin, and S. M. Selbach, MRS Commun. **6**, 182 (2016).
[11] R. L. Johnson-Wilke, D. Marincel, S. Zhu, M. P. Warusawithana, A. Hatt, J. Sayre, K. T. Delaney, R. Engel-Herbert, C. M. Schlepuetz, J. W. Kim *et al.*, Phys. Rev. B **88**, 174101, 174101 (2013).
[12] K. M. Rabe, Curr. Opin. Solid State Mater. Sci. **9**, 122 (2005).
[13] J. Chakhalian, A. J. Millis, and J. Rondinelli, Nat. Mater. **11**, 92 (2012); I. Hallsteinsen, J. E. Boschker, M. Nord, S. Lee, M. Rzchowski, P. E. Vullum, J. K. Grepstad, R. Holmestad, C. B. Eom, and T. Tybell, J. Appl. Phys. **113**, 183512, 183512 (2013).
[14] D. Doennig, W. E. Pickett, and R. Pentcheva, Phys. Rev. Lett. **111**, 126804 (2013); S. Middey, D. Meyers, D. Doennig, M. Kareev, X. Liu, Y. Cao, Z. Yang, J. Shi, L. Gu, P. J. Ryan *et al.*, Phys. Rev. Lett. **116**, 056801 (2016); S. Raghu, X. L. Qi, C. Honerkamp, and S. C. Zhang, Phys Rev Lett **100**, 156401 (2008); D. Xiao, W. Zhu, Y. Ran, N. Nagaosa, and S. Okamoto, Nat. Commun. **2**, 596 (2011); K.-Y. Yang, W. Zhu, D. Xiao, S. Okamoto, Z. Wang, and Y. Ran, Phys. Rev. B **84**, 201104 (2011).
[15] T. H. Kim, D. Puggioni, Y. Yuan, L. Xie, H. Zhou, N. Campbell, P. J. Ryan, Y. Choi, J. W. Kim, J. R. Patzner *et al.*, Nature **533**, 68 (2016).
[16] Y. B. Xu, Y. L. Tang, Y. L. Zhu, Y. Liu, S. Li, S. R. Zhang, and X. L. Ma, Sci. Rep. **6**, 35172 (2016).
[17] J. F. Li, J. L. Wang, M. Wuttig, R. Ramesh, N. Wang, B. Ruette, A. P. Pyatakov, A. K. Zvezdin, and D. Viehland, Appl. Phys. Lett. **84**, 5261 (2004).
[18] M. Moreau, A. Marthinsen, S. M. Selbach, and T. Tybell, Phys. Rev. B **95**, 064109 (2017).
[19] A. Raeliarijaona and H. X. Fu, J. Appl. Phys. **115**, 054105 (2014).
[20] R. Oja, K. Johnston, J. Frantti, and R. M. Nieminen, Phys. Rev. B **78**, 094102 (2008).
[21] A. J. Grutter, A. Vailionis, J. A. Borchers, B. J. Kirby, C. L. Flint, C. He, E. Arenholz, and Y. Suzuki, Nano Lett. **16**, 5647 (2016); Z. Liao, M. Huijben, Z. Zhong, N. Gauquelin, S. Macke, R. J. Green, S. Van Aert, J. Verbeeck, G. Van Tendeloo, K. Held *et al.*, Nat. Mater. **15**, 425 (2016).
[22] I. Hallsteinsen, M. Moreau, A. Grutter, M. Nord, P. E. Vullum, D. A. Gilbert, T. Bolstad, J. K. Grepstad, R. Holmestad, S. M. Selbach *et al.*, Phys. Rev. B **94**, 201115 (2016).
[23] J. M. Rondinelli and C. J. Fennie, Adv. Mat. **24**, 1961 (2012).
[24] J. Hong, A. Stroppa, J. Íñiguez, S. Picozzi, and D. Vanderbilt, Phys. Rev. B **85**, 054417 (2012).
[25] V. M. Goldschmidt, Die Naturwissenschaften **14**, 477 (1926).
[26] R. J. Angel, J. Zhao, and N. L. Ross, Phys. Rev. Lett. **95**, 025503 (2005); J. Zhao, N. L. Ross, and R. J. Angel, J. Phys.: Condens. Matter **16**, 8763 (2004); T. Tohei, A. Kuwabara, T. Yamamoto, F. Oba, and I.

Tanaka, Phys. Rev. Lett. **94**, 035502 (2005); J. Zhao, N. L. Ross, and R. J. Angel, Acta Crystallogr. Sect. B **62**, 431 (2006).
[27] K. A. Muller, W. Berlinger, and F. Waldner, Phys. Rev. Lett. **21**, 814 (1968).
[28] M. Marezio, P. D. Dernier, and J. P. Remeika, J. Solid State Chem. **4**, 11 (1972).
[29] I. K. Bdikin, I. M. Shmyt'ko, A. M. Balbashov, and A. V. Kazansky, J. Appl. Crystallogr. **26**, 71 (1993).
[30] S. Geller, Acta Crystallogr. **10**, 243 (1957).
[31] M. Eibschütz, S. Shtrikman, and D. Treves, Phys. Rev. **156**, 562 (1967); S. Geller and P. M. Raccah, Phys. Rev. B **2**, 1167 (1970).
[32] R. Diehl and G. Brandt, Mater. Res. Bull. **10**, 85 (1975).
[33] R. P. Liferovich and R. H. Mitchell, J. Solid State Chem. **177**, 2188 (2004).
[34] G. H. Kwei, A. C. Lawson, S. J. L. Billinge, and S. W. Cheong, J. Phys. Chem. **97**, 2368 (1993).
[35] L. Rimai and G. A. deMars, Phys. Rev. **127**, 702 (1962).
[36] D. M. Helen, Proc. Phys. Soc. **58**, 133 (1946).
[37] H. F. Kay and P. C. Bailey, Acta Crystallogr. **10**, 219 (1957).
[38] L. Carlsson, Acta Crystallogr. **23**, 901 (1967).
[39] A. W. Hewat, J. Phys. C: Solid State Phys. **6**, 2559 (1973).
[40] G. A. Samara and B. Morosin, Phys. Rev. B **8**, 1256 (1973); C. H. Perry and T. F. McNelly, Phys. Rev. **154**, 456 (1967).
[41] M. Ahtee and C. N. W. Darlington, Acta Crystallogr B **36**, 1007 (1980).
[42] S. K. Mishra, N. Choudhury, S. L. Chaplot, P. S. R. Krishna, and R. Mittal, Phys. Rev. B **76**, 024110 (2007).
[43] M. Yashima, S. Matsuyama, R. Sano, M. Itoh, K. Tsuda, and D. Fu, Chem. Mater. **23**, 1643 (2011).
[44] B. A. Wechsler and R. B. Von Dreele, Acta Crystallogr. Sect. B **45**, 542 (1989).
[45] S. C. Abrahams, J. M. Reddy, and J. L. Bernstein, J. Phys. Chem. Solids **27**, 997 (1966).
[46] G. Kresse and J. Furthmuller, Phys. Rev. B **54**, 11169 (1996).
[47] G. Kresse and D. Joubert, Phys. Rev. B **59**, 1758 (1999).
[48] P. E. Blochl, Phys. Rev. B **50**, 17953 (1994).
[49] J. P. Perdew, A. Ruzsinszky, G. I. Csonka, O. A. Vydrov, G. E. Scuseria, L. A. Constantin, X. Zhou, and K. Burke, Phys. Rev. Lett. **100**, 136406, 136406 (2008).
[50] W. C. Koehler and E. O. Wollan, J. Phys. Chem. Solids **2**, 100 (1957).
[51] VASP manual, https://cms.mpi.univie.ac.at/vasp/vasp/vasp.html (2017).
[52] S. L. Dudarev, G. A. Botton, S. Y. Savrasov, C. J. Humphreys, and A. P. Sutton, Phys. Rev. B **57**, 1505 (1998).
[53] K. Kunc and R. M. Martin, Phys. Rev. Lett. **48**, 406 (1982).
[54] A. Togo and I. Tanaka, Scr. Mater. **108**, 1 (2015).
[55] K. Momma and F. Izumi, J. Appl. Crystallogr. **44**, 1272 (2011).
[56] See Supplemental Material at [URL will be inserted by publisher] for discussion about the octahedral distortions, data for the supplementing materials, relative eigenvalue amplitude of $NaTaO_3$ and in-plane polar mode analysis.
[57] Tolerance Factor Calculator, http://www.me.utexas.edu/~benedekgroup/ToleranceFactorCalculator/ (Accessed 20.01 2017).
[58] A. Vailionis, H. Boschker, W. Siemons, E. P. Houwman, D. H. A. Blank, G. Rijnders, and G. Koster, Phys. Rev. B **83**, 064101 (2011).
[59] E. Bousquet and P. Ghosez, Phys. Rev. B **74**, 180101 (2006).
[60] H. J. Xiang, M. Guennou, J. Íñiguez, J. Kreisel, and L. Bellaiche, Phys. Rev. B **96**, 054102 (2017).
[61] J. Young and J. M. Rondinelli, J. Phys. Chem. Lett. **7**, 918 (2016).

Figures

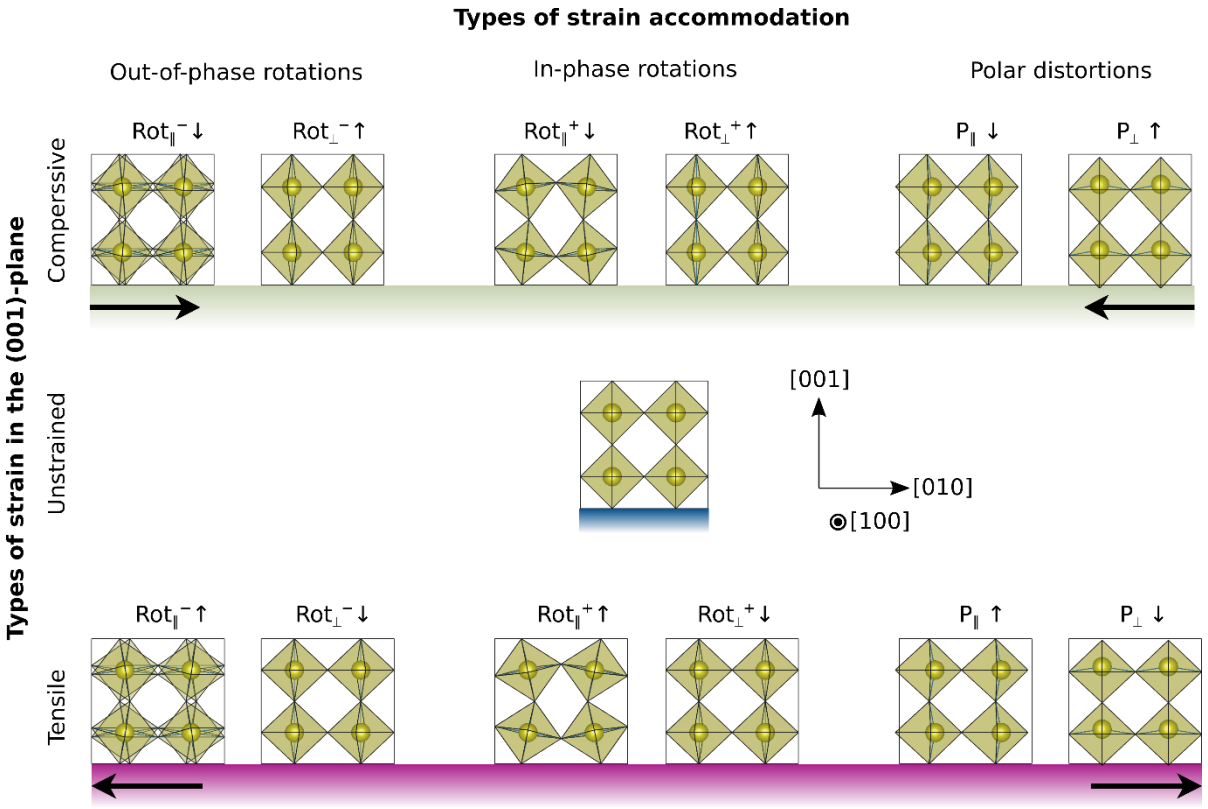

Figure 1: Strain-phonon coupling for (001)-strain. The sketches show the different phonon modes in $2 \times 2 \times 2$, supercells, A cations and oxygen atoms omitted for clarity. The modes discussed in this paper are out-of-phase rotations denoted Rot^{-}, In-phase rotations denoted Rot^{+} and polar distortions of the B-cation denoted *P*. Subscript ∥ and ⊥ denotes in-plane and out-of-plane modes respectively. Arrow up (down) denotes that the preceding mode type is softer (harder) for that type of strain.

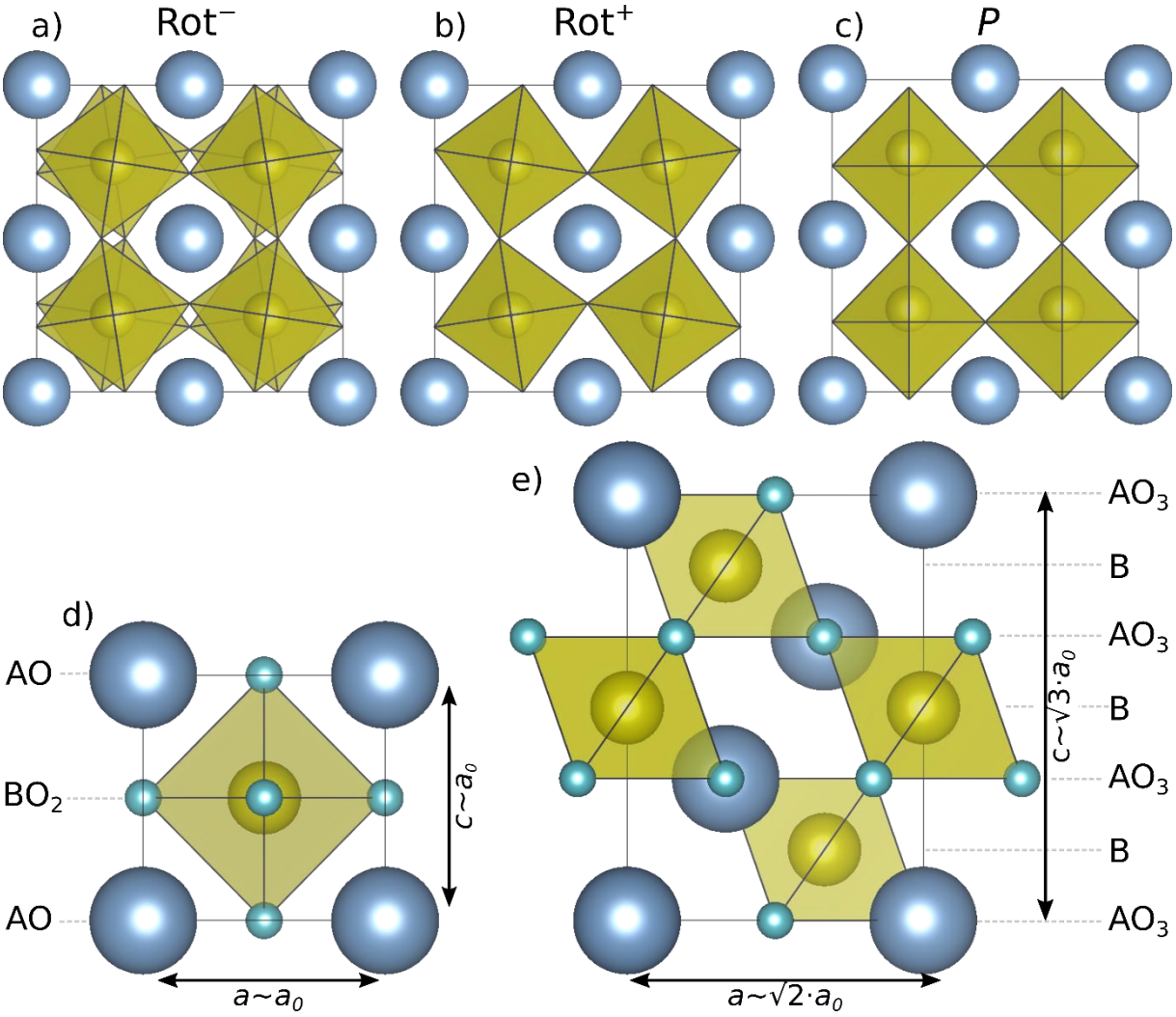

Figure 2: a), b) and c) depicts three important phonon modes for perovskite oxides, here depicted in $2 \times 2 \times 2$ supercells which were used for the phonon calculations. a) Visualization of the out-of-phase rotations at the *R*-point of the Brillouin zone, denoted Rot^{-}. b) Visualization of the in-phase rotations at the *M*-point of the Brillouin zone, denoted Rot^{+}. c) Visualization of the polar distortions of the B-cation at Γ-point of the Brillouin zone, denoted *P*. In a-c) the oxygen atoms are omitted for clarity. d) and e) calculation cells used for (001)- and (111)-strain respectively, along with the relations between the lattice vectors and the stacking sequence.

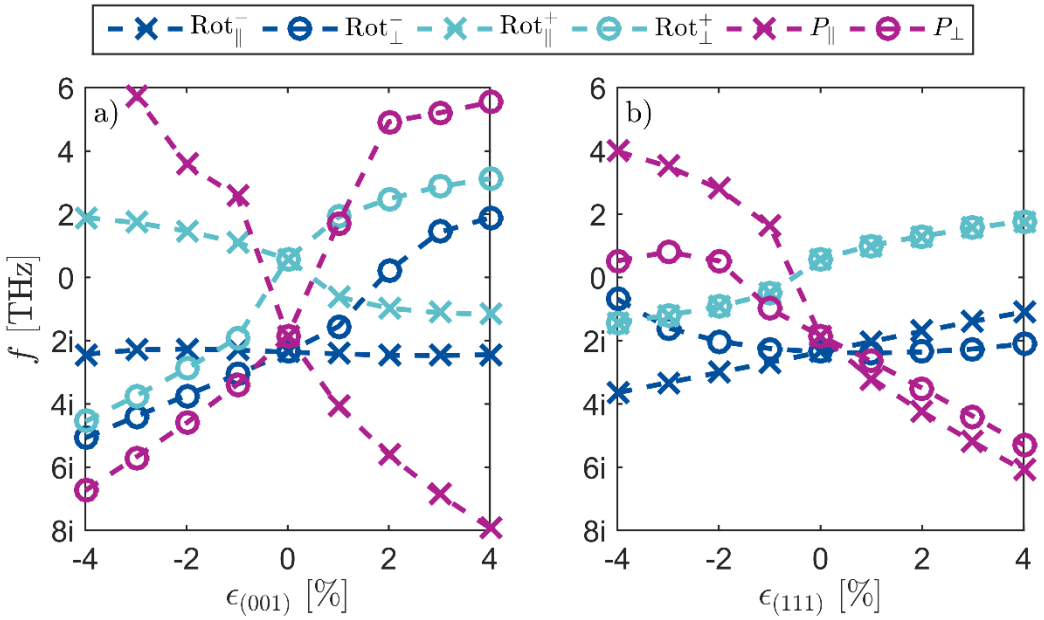

Figure 3: The frequencies of the three different phonon modes considered as a function of in-plane strain in the a) (001)-plane and b) (111)-plane for $SrTiO_3$ (STO). Under strain the phonon frequencies are split into two degenerate perpendicular in-plane modes denoted with a subscript ∥, and one out-of-plane mode denoted with a subscript ⊥. The three different modes considered are out-of-phase rotations denoted by Rot^{-}, in-phase rotations denoted by Rot^{+} and polar displacement of the B-cation denoted by P. For (001)-strain the in-plane directions are [100] and [010], while the out-of-plane direction is [001]. For (111)-strain the in-plane directions are $[1\bar{1}0]$ and $[11\bar{2}]$ while the out-of-plane direction is [111]. The dashed lines are guides to the eye.

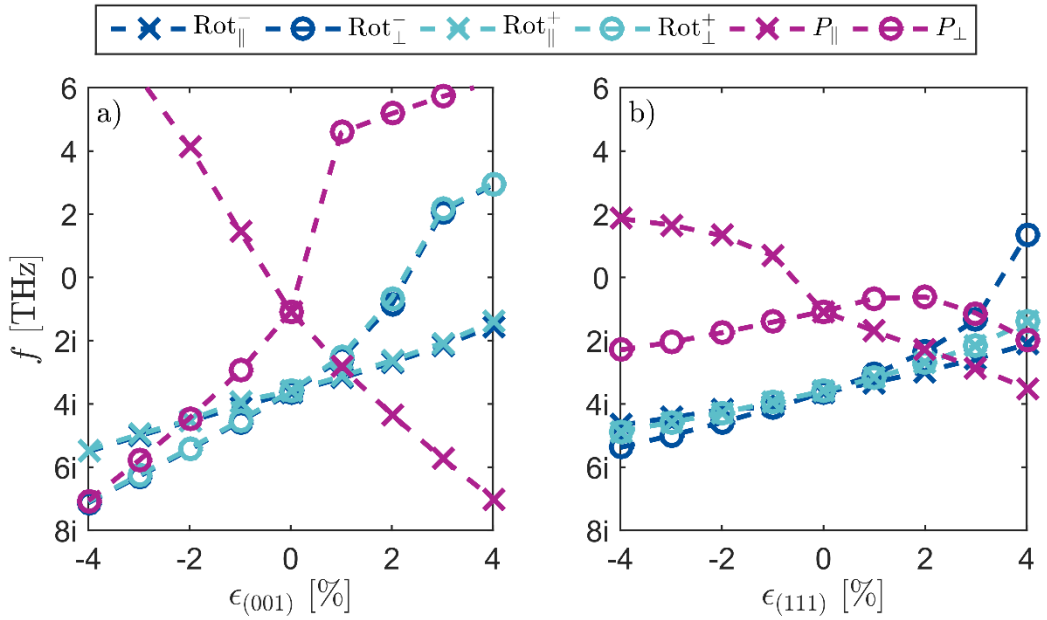

Figure 4: The frequencies of the three different phonon modes considered as a function of in-plane strain in the a) (001)-plane and b) (111)-plane for $NaTaO_3$ (NTO). Under strain the phonon frequencies are split into two degenerate perpendicular in-plane modes denoted with a subscript ∥, and one out-of-plane mode denoted with a subscript ⊥. The three different modes considered are out-of-phase rotations denoted by Rot^-, in-phase rotations denoted by Rot^+ and polar displacement of the B-cation denoted by P. For (001)-strain the in-plane directions are [100] and [010], while the out-of-plane direction is [001]. For (111)-strain the in-plane directions are $[1\bar{1}0]$ and $[11\bar{2}]$ while the out-of-plane direction is [111]. The dashed lines are guides to the eye.

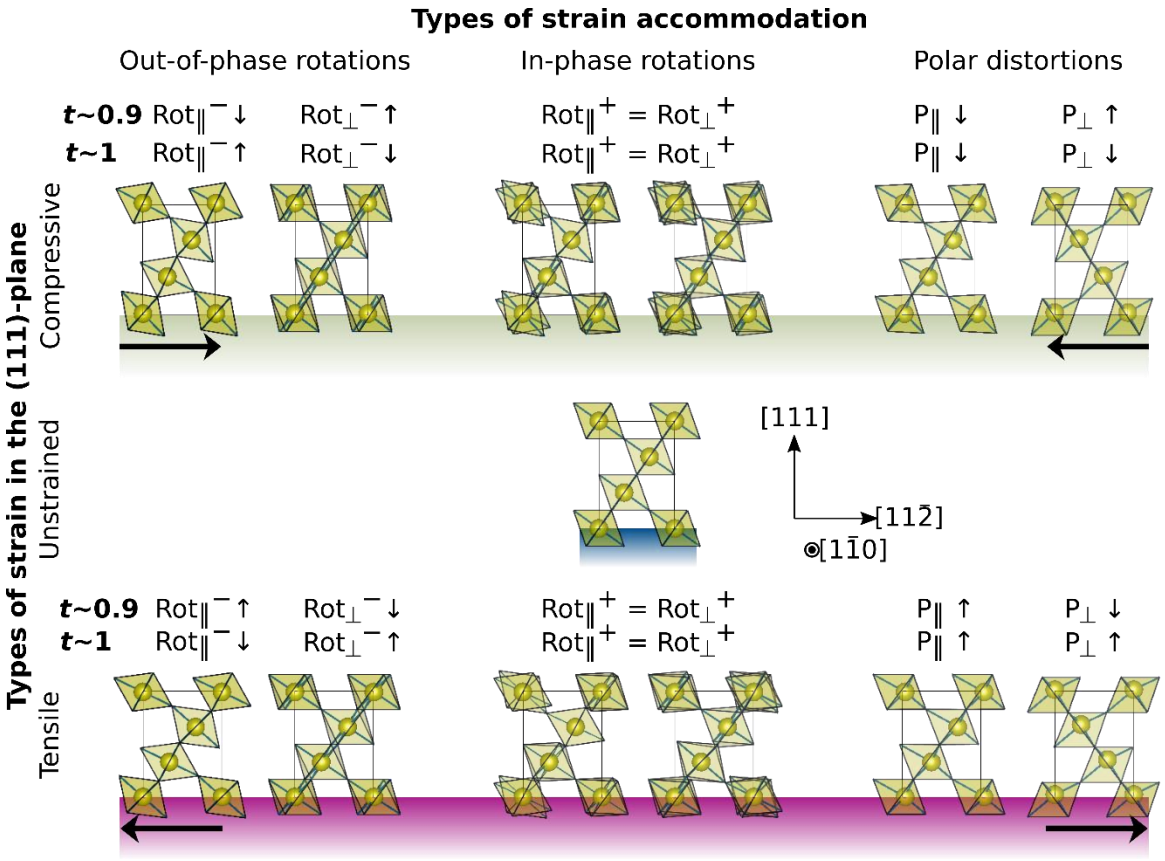

Figure 5: Strain-phonon coupling for (111)-strain. The schematic shows the different phonon modes in $\sqrt{2} \times \sqrt{2} \times \sqrt{3}$, supercells, A cations and oxygen omitted for clarity. Arrow up (down) denotes that the preceding mode type is softer (harder) for that type of strain. The strain-phonon coupling for (111)-strain is different for high ($t \sim 1$) and low ($t \sim 0.9$) tolerance factors, as discussed in the text. The exact crossover depends on the relative charge of the A- and B- cations. For low tolerance factors, the response is similar to what is known for (001)-strain, except for in-plane rotations, which are not split for (111)-strain, while for high tolerance factors, different responses are seen.

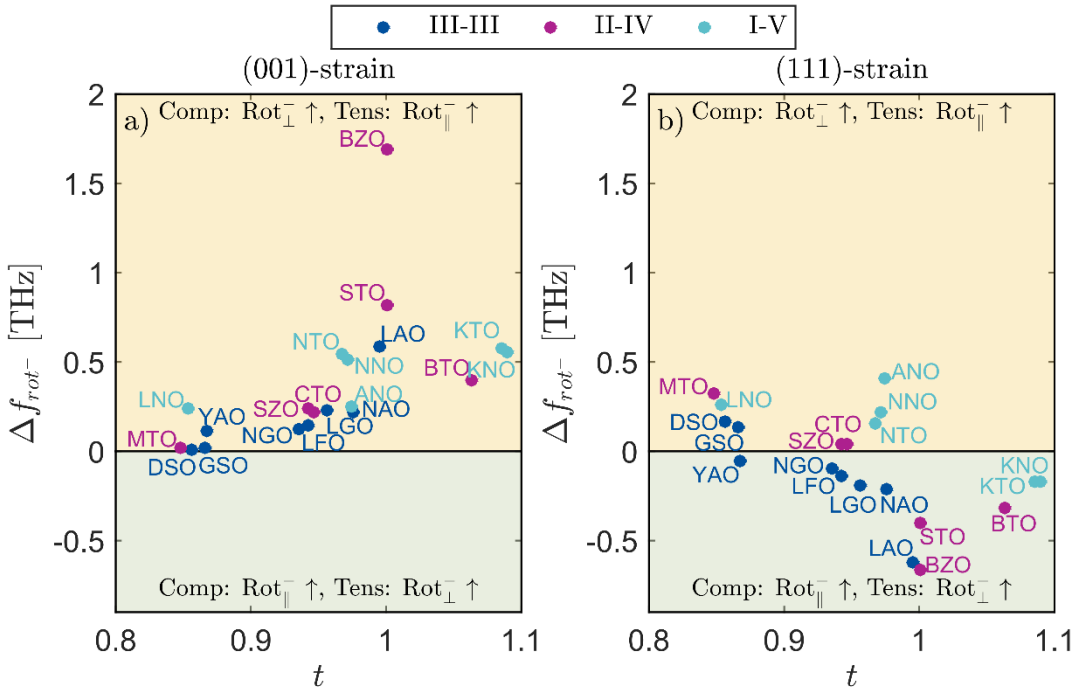

Figure 6: The degree of splitting, Δf_{rot-} between in-plane and out-of-plane out-of-phase rotations as a function for $\pm$1% a) (001)-strain and b) (111)-strain as a function of tolerance factor t. A positive Δf_{rot-}, yellow area, indicates (001)-like splitting where out-of-plane rotations are softer for compressive (comp) strain and out-of-plane rotations are softer for tensile (tens) strain. In the green area an opposite splitting is seen, where in-plane rotations are softer for comp strain, and out-of-plane rotations are softer for tens strain. See Table I for abbreviations.

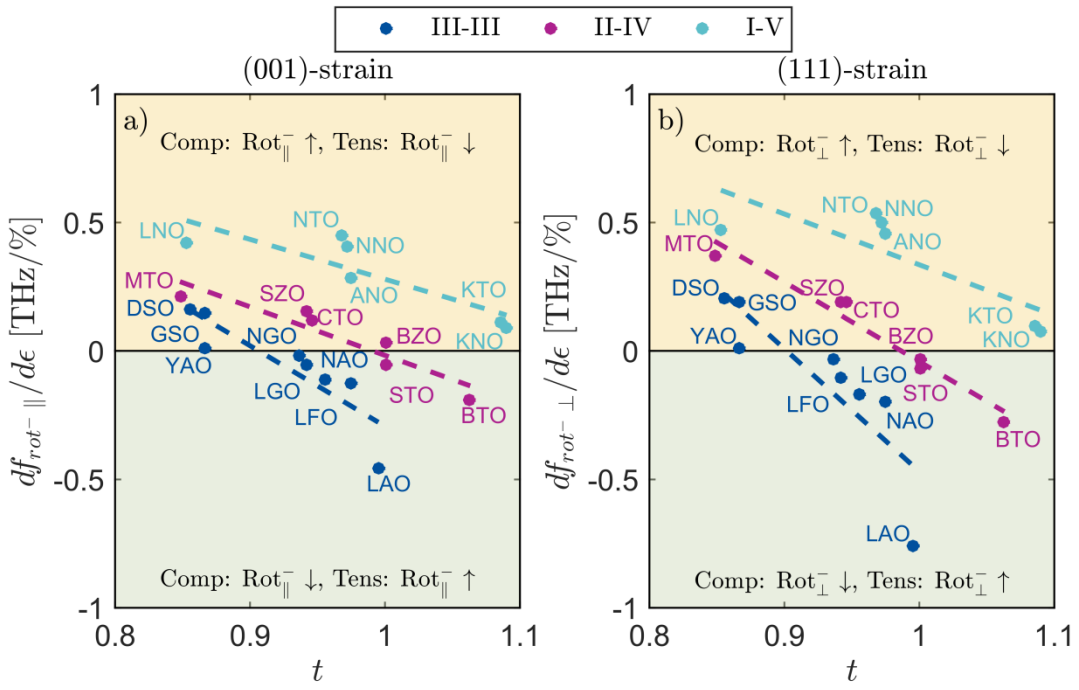

Figure 7: Derivative of the in-plane out-of-phase rotational modes with respect to a) (001)-strain and b) (111)-strain. A positive $df/d\epsilon$, yellow area, means that the respective mode is softened by compressive (comp) strain and hardened by tensile (tens) strain, while a negative $df/d\epsilon$, green area, means that the respective mode is softened tens strain and hardened for comp strain and softened for tens strain. See Table I for abbreviations. The dashed lines are guides to the eye, based on linear fits to the data.

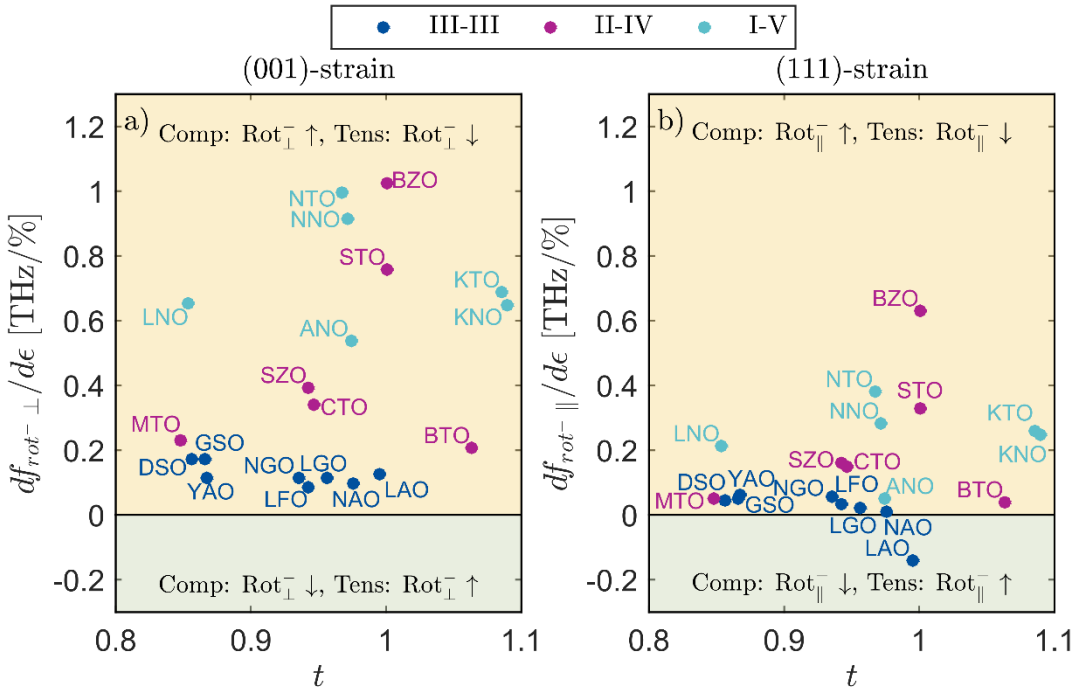

Figure 8: Derivative of the out-of-plane out-of-phase rotational modes with respect to a) (001)-strain and b) (111)-strain. A positive $df/d\epsilon$, yellow area, means that the respective mode is softened by compressive (comp) strain and hardened by tensile (tens) strain, while a negative $df/d\epsilon$, green area, means that the respective mode is softened tens strain and hardened for comp strain and softened for tens strain. See Table I for abbreviations. No trend lines are added, as no given trend is seen.

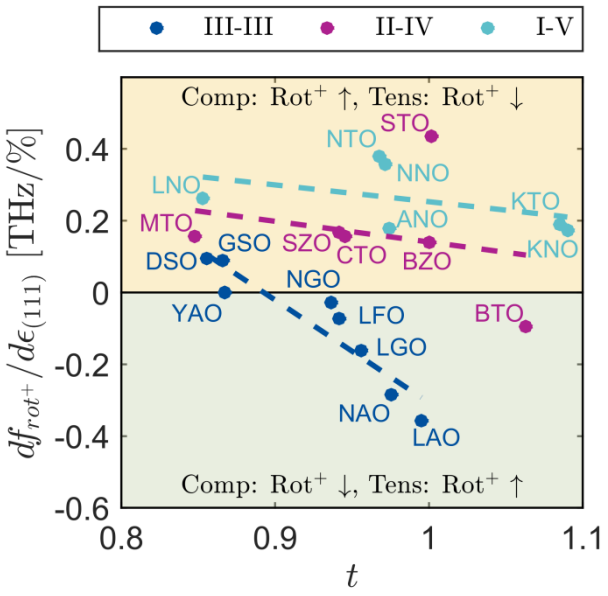

Figure 9: Derivative of the in-phase rotational modes with respect to (111)-strain as a function of tolerance factor, t. Note that since the in-phase rotations are not split under (111)-strain, this plot shows both in-plane and out-of-plane modes, as they are degenerate. A positive $df/d\epsilon$, yellow area, means that the respective mode is softened by compressive (comp) strain and hardened by tensile (tens) strain, while a negative $df/d\epsilon$, green area, means that the respective mode is softened by tens strain and hardened for comp strain and softened for tens strain. See Table I for abbreviations. The dashed lines are guides to the eye, based on linear fits to the data.

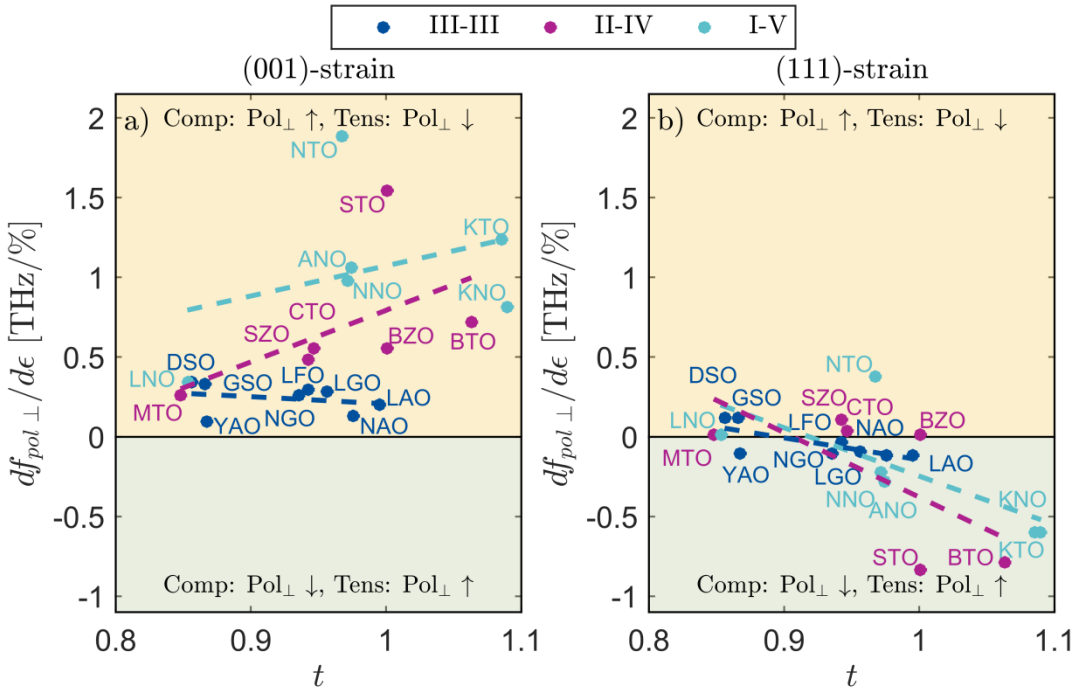

Figure 10: Derivative of the out-of-plane polar modes as a function of tolerance factor t with respect to a) (001)-strain and b) (111)-strain as a function of tolerance factor t. A positive $df/d\epsilon$, yellow area, means that the respective mode is softened by compressive (comp) strain and hardened by tensile (tens) strain, while a negative $df/d\epsilon$, green area, means that the respective mode is softened by tens strain and hardened for comp strain and softened for tens strain. See Table I for abbreviations. . The dashed lines are guides to the eye, based on linear fits to the data.

Table I: Tolerance factor, t,[57] relaxed lattice constant a_0 in the aristotype cubic phases, and Poisson's ratio, ν, for (001)- and (111)-strain for the material systems studied. The table is sorted first with respect to the oxidation state of the A and B cations, then after declining tolerance factor.

Material system	abbreviation	t	a_0 [Å]	$\nu_{(001)}$	$\nu_{(111)}$
		III-III			
$LaAlO_3$	LAO	0.995	3.800	0.272	0.184
$NdAlO_3$	NAO	0.975	3.734	0.250	0.193
$LaGaO_3$	LGO	0.956	3.890	0.275	0.245
$LaFeO_3$	LFO	0.942	3.912	0.272	0.277
$NdGaO_3$	NGO	0.936	3.835	0.258	0.261
$YAlO_3$	YAO	0.867	3.676	0.231	0.214
$GdScO_3$	GSO	0.866	3.976	0.160	0.333
$DyScO_3$	DSO	0.856	3.967	0.157	0.340
		II-IV			
$BaTiO_3$	BTO	1.063	3.984	0.260	0.213
$SrTiO_3$	STO	1.001	3.895	0.228	0.245
$BaZrO_3$	BZO	1.000	4.190	0.206	0.273
$CaTiO_3$	CTO	0.946	3.844	0.216	0.279
$SrZrO_3$	SZO	0.942	4.133	0.180	0.303
$MgTiO_3$	MGO	0.848	3.802	0.229	0.331
		I-V			
$KNbO_3$	KNO	1.090	3.986	0.155	0.286
$KTaO_3$	KTO	1.085	3.989	0.146	0.290
$AgNbO_3$	ANO	0.974	3.948	0.202	0.382
$NaNbO_3$	NNO	0.972	3.942	0.144	0.326
$NaTaO_3$	NTO	0.968	3.949	0.134	0.329
$LiNbO_3$	LNO	0.853	3.922	0.143	0.349